J. Fluid Mech. (1997), *vol.* 331, *pp.* 261–282

Degenerate bifurcation in stably stratified plane Poiseuille flow

By K. FUJIMURA[1] AND R. E. KELLY[2]

[1]Japan Atomic Energy Research Institute, Tokai-mura, Ibaraki 319-11, Japan

[2]Mechanical and Aerospace Engineering Department, University of California, Los Angeles, CA 90095-1597, USA

(Received 6 November 1995 and in revised form 21 August 1996)

Bifurcation characteristics of stably stratified plane Poiseuille flow have been investigated on a weakly nonlinear basis. It is found that the results are sensitive to the value of the Prandtl number, in that subcritical bifurcation persists for most values of the Prandtl number but is replaced by supercritical bifurcation over a range of small values of the Prandtl number. This range includes values characteristic of some liquid metals. The bifurcation becomes degenerate at a particular parameter set where the real part of the cubic nonlinear coefficient in the Stuart–Landau equation vanishes at criticality, and the situation is discussed by including higher-order terms in the manner of Eckhaus & Iooss (1989). An exact hyper-degenerate situation is also found to be possible for which the cubic and the quintic nonlinear coefficients lose their real parts simultaneously; this case is also analysed. For large values of the Prandtl number, stable stratification tends to promote subcritical instability.

1. Introduction

Weakly nonlinear evolution of a single-wavenumber disturbance added to a basic fluid motion is described by the Stuart–Landau equation if the fundamental mode is neutrally stable and all the harmonics as well as the zeroth harmonic are stable:

$$\frac{\mathrm{d}A}{\mathrm{d}t} = \sigma A + \sum_j \lambda_j |A|^{2j} A,$$

where λ_j is called the jth Landau constant. In the usual situation, the Stuart–Landau equation can be truncated at the cubic-order approximation. If the real part of the first Landau constant λ_1 stays negative along the neutral stability curve, as is the case for Rayleigh–Bénard convection or Taylor–Couette flow, the bifurcation is supercritical so that the nonlinear evolution of the disturbance occurs smoothly to an asymptotic value as $t \to \infty$.

On the other hand, if the real part of λ_1 is positive, subcritical instability occurs. The bifurcation diagram for the subcritical situation consists of a curve that stems from the linear neutral stability curve, $(\alpha, Re_n(\alpha))$ say, into the subcritical region $(Re < Re_n(\alpha))$, which we refer to as the lower branch of the bifurcation diagram, and then bends back towards the supercritical region $(Re > Re_n(\alpha))$, which we refer to as the upper branch of the bifurcation diagram. Plane Poiseuille flow is a typical example which exhibits a subcritical feature at the linear critical point. Reynolds & Potter (1967) and Pekeris & Shkoller (1967) pointed out that the sign of the first

Landau constant changes from negative to positive if we trace the neutral stability curve from the lower branch to the upper branch. We call a situation degenerate when $\mathrm{Re}\lambda_1$ changes its sign. In plane Poiseuille flow, a degenerate situation occurs at $(\alpha, Re) \simeq (0.9067, 6842)$ on the neutral stability curve where α is the wavenumber and Re is the Reynolds number. For this flow, the upper branch of the bifurcation diagram has a large amplitude when $\alpha \gg 0.9067$. Therefore, the branch is outside the radius of convergence of the Stuart–Landau equation as has been pointed out, for example, by Herbert (1980). In a neighbourhood of the degenerate situation, on the other hand, the Stuart–Landau equation might describe the dynamics both along the upper branch and the lower branch of the bifurcation diagram. Therefore, study of the degenerate situation might help us to get a qualitative image of the equilibrium solutions along the upper branch of the bifurcation diagram.

Eckhaus & Iooss (1989) investigated systematically the degenerate bifurcation problem. They showed how the bifurcation of the non-degenerate case is affected by the degeneracy, examined the stability of periodic solutions subject to general perturbations, and considered a hyper-degenerate situation where the real parts of λ_j for $j = 1, 2, \cdots$ vanish simultaneously. As a prototype of the hyper-degenerate situation, they referred to Sen & Vashist's (1989) numerical results on the Blasius boundary layer where $\mathrm{Re}\lambda_1$, $\mathrm{Re}\lambda_2$, and $\mathrm{Re}\lambda_3$ vanish almost simultaneously (although not at Re_c).

Degenerate bifurcation is known to occur at the linear critical point in a couple of flow fields. Among them, Taylor–Couette flow between counter-rotating cylinders was investigated by Laure & Demay (1988). In this problem, with a specific ratio of outer/inner rotation speeds, the critical disturbance suffers from degeneracy. They applied the center manifold reduction and derived the Stuart–Landau equation with a quintic nonlinear term. A similar situation for double-diffusive convection was investigated by Knobloch (1986). Under free–free boundary conditions, degenerate Hopf bifurcation is encountered in the presence of O(2) symmetry. Knobloch derived coupled amplitude equations with quintic nonlinear terms and classified the bifurcation characteristics.

Since plane Poiseuille flow already has a degenerate point on the neutral stability curve, we should be able to arrange for the degenerate situation to occur at the critical point by adjusting an additional control parameter. If one appropriate parameter is introduced, $\mathrm{Re}\lambda_1$ can vanish at the critical point, in principle. If two appropriate parameters are introduced, then $\mathrm{Re}\lambda_1$ and $\mathrm{Re}\lambda_2$ can vanish simultaneously at the critical point, exhibiting a hyper-degenerate situation.

In the present paper, we investigate stably stratified plane Poiseuille flow in a horizontal channel of infinite extent in both horizontal directions. The linear stability of the flow is well understood (e.g. Gage & Reid 1968 and Tveitereid 1974). There are three control parameters in the problem, i.e. the Reynolds number, Prandtl number P, and the Richardson number Ri (or Rayleigh or Grashof number). Consider the linear critical situation. For prescribed (P, Ri), α and Re are determined uniquely because of the criticality requirement. Therefore we have two free parameters P and Ri. We shall show that the degenerate situation $\mathrm{Re}\lambda_1 = 0$ sets in along a curve in the (P, Ri)-plane for $P \leqslant 0.17$ (which includes mercury). We shall also show that $\mathrm{Re}\lambda_1 = \mathrm{Re}\lambda_2 = 0$ for one specific parameter set. The real part of the third Landau constant also changes its sign in the close vicinity of the critical point, thus exhibiting the hyper-degenerate situation. We shall evaluate the Landau constants of the Stuart–Landau equation numerically and then discuss the number of bifurcated solutions based on the actual numerical coefficients.

A low Prandtl number is intrinsic for most liquid metals. Liquid metals have been attracting much attention as effective coolants for heat transfer devices like the fusion Tokamak machine, the inertia confinement fusion machine, and the fast breeder fission reactor. For example, liquid lithium, Li17Pb83, and lead have been considered as the coolant for the liquid breeder blanket, whereas liquid lithium, gallium, and sodium have been considered for the divertor in fusion reactor designs, and liquid lead and liquid FLiBe have been considered for inertia confinement fusion reactors. Liquid sodium has been utilized as a coolant in fast breeder fission reactors. In some cases, turbulent flow is preferred, whereas in other cases, laminar flow is preferred. Therefore, the stability characteristics of the basic flow is a critical issue for the integrity of the design. Although plane Poiseuille flow is too simplified a configuration for us to predict heat transfer characteristics of practical devices, the stability/bifurcation characteristics obtained in the present paper will help us to understand flow properties in more practical applications. There are indeed many liquid metal experimental apparatuses having rectangular test sections with relatively large aspect ratio (e.g. Kirillov, Reed & Barleon 1995), which may be relevant to the present work.

2. Mathematical formulation

We assume a plane Poiseuille flow in a horizontal channel whose top and bottom walls located at $z^* = \pm H$ are respectively heated and cooled at uniform temperatures $T_0 + \Delta T$ and $T_0 - \Delta T$, where $\Delta T > 0$. The flow is in the x-direction. The motion of fluid and temperature (assuming a Boussinesq fluid) are governed by

$$\left.\begin{aligned} \rho[\partial_{t^*}\boldsymbol{v}^* + (\boldsymbol{v}^*\cdot\nabla^*)\boldsymbol{v}^*] &= -\nabla^* p^* - \rho g[1-\beta(T^*-T_0)]\boldsymbol{e}_z^* + \mu\nabla^{*2}\boldsymbol{v}^*, \\ \partial_{t^*}T^* + (\boldsymbol{v}^*\cdot\nabla^*)T^* &= \kappa\nabla^{*2}T^*, \\ \nabla^*\cdot\boldsymbol{v}^* &= 0, \end{aligned}\right\} \tag{1}$$

where $\boldsymbol{v}^*$ is the velocity, T^* is the temperature, p^* is the pressure, ρ is the density, g is the acceleration due to gravity, β is the thermal expansion coefficient, μ is the viscosity, and κ is the thermal diffusivity. The asterisk denotes a dimensional quantity. We non-dimensionalize all the quantities as

$$\boldsymbol{v}^* = \bar{u}_0\boldsymbol{v}, \quad \boldsymbol{x}^* = H\boldsymbol{x}, \quad T^* = \Delta T\cdot T, \quad t^* = H\bar{u}_0^{-1}t, \quad \text{and} \quad p^* = \rho_0\bar{u}_0^2 p,$$

where $\bar{u}_0$ is the maximum velocity on the centreline of a channel and ρ_0 is the density evaluated at a reference temperature T_0.

Split $\boldsymbol{v}$, T, and p into the basic field (with overbar) and the disturbance (with overhat) as

$$\boldsymbol{v}(x,y,z;t) = \bar{\boldsymbol{v}}(z) + \hat{\boldsymbol{v}}(x,y,z;t), \quad T(x,y,z;t) = \bar{T}(z) + \hat{T}(x,y,z;t),$$

$$\text{and} \quad p(x,y,z;t) = \bar{p}(z) + \hat{p}(x,y,z;t).$$

The basic field is easily obtained as

$$\bar{\boldsymbol{v}} = (\bar{u},0,0) = (1-z^2,0,0), \quad \bar{T} = z. \tag{2}$$

In unstably stratified plane Poiseuille flow, a buoyancy-driven mode consisting of longitudinal rolls having their axes parallel to the shear flow or a hydrodynamic instability mode consisting of transverse travelling waves, i.e. Tollmien–Schlichting waves, gives the critical condition depending on the parameters. Therefore, three-dimensionality of the disturbance should be taken into account to clarify the stability

characteristics (Fujimura & Kelly 1995, for example.) In the present paper, on the other hand, the stably stratified situation never excites a buoyancy-driven instability mode. We thus focus on purely two-dimensional disturbances in the (x, z)-plane added to the two-dimensional basic field. We introduce the stream function for the disturbance, $\hat{\psi}(x, z; t)$, such that

$$\hat{u} = \partial\hat{\psi}/\partial z, \quad \hat{w} = -\partial\hat{\psi}/\partial x.$$

The disturbance components are thus described by the equations

$$\left.\begin{aligned} \partial_t \nabla^2\hat{\psi} + \bar{u}\partial_x\nabla^2\hat{\psi} - \bar{u}''\hat{\psi}_x = Re^{-1}\nabla^4\hat{\psi} - Ri\hat{T}_x + J(\hat{\psi}, \nabla^2\hat{\psi}), \\ \hat{T}_t + \bar{u}\hat{T}_x - \hat{\psi}_x = Re^{-1}P^{-1}\nabla^2\hat{T} + J(\hat{\psi}, \hat{T}), \end{aligned}\right\} \tag{3}$$

where we have three non-dimensional parameters: $Re = \rho_0 u_o H/\mu$ is the Reynolds number, $P = \mu/(\rho_0\kappa)$ is the Prandtl number, and $Ri = RaRe^{-2}P^{-1}$ is the Richardson number which is related to the Rayleigh number $Ra = \beta g \Delta T H^3/(\mu\kappa)$; we define ΔT so $Ra > 0$ for heating from above. $J(f, g)$ is the Jacobian defined by $\partial(f, g)/\partial(x, z)$, and the prime indicates differentiation with respect to z.

The boundary conditions for $\hat{\psi}$ and $\hat{T}$ are imposed as

$$\hat{\psi} = \partial\hat{\psi}/\partial z = 0 \quad \text{and} \quad \hat{T} = 0 \quad \text{at} \quad z = \pm 1. \tag{4}$$

3. Linear critical conditions

Before discussing the weakly nonlinear problem, let us first describe the linear critical conditions for a wide parameter range. For this purpose, we apply the normal mode analysis simply assuming that

$$\begin{pmatrix} \hat{\psi} \\ \hat{T} \end{pmatrix} = \begin{pmatrix} \phi(z) \\ \theta(z) \end{pmatrix} \mathrm{e}^{\mathrm{i}\alpha(x-ct)}. \tag{5}$$

Substitution of this expression into the linearized version of the disturbance equations (3) and the boundary conditions (4) yields

$$\left.\begin{aligned} [\mathrm{i}\alpha(\bar{u} - c)S - \mathrm{i}\alpha\bar{u}'' - Re^{-1}S^2]\phi + \mathrm{i}\alpha Ri\theta = 0, \\ -\mathrm{i}\alpha\phi + [\mathrm{i}\alpha(\bar{u} - c) - Re^{-1}P^{-1}S]\theta = 0, \end{aligned}\right\} \tag{6}$$

and the homogeneous boundary conditions

$$\phi = \mathrm{D}\phi = \theta = 0 \quad \text{at} \quad z = \pm 1, \tag{7}$$

where $S = \mathrm{D}^2 - \alpha^2$ and $\mathrm{D} = \mathrm{d}/\mathrm{d}z$.

We solve the linear eigenvalue problem consisting of (6) and (7) by an expansion of $[\phi, \theta]^T$ into Chebyshev polynomials. Since the numerical scheme for the Chebyshev collocation method is now routine (see Fujimura & Kelly 1995, for example) we skip the details and give the final numerical results below.

We have compared the critical conditions (Re_c, Ri_c) for $P = 1$ with the Gage & Reid (1968) asymptotic results which are valid for $Re \gg 1$. Although we do not demonstrate the comparison in order to save space, our numerical values agree well with theirs for $Re < 5 \times 10^4$ whereas a numerical difficulty prevents our obtaining the critical conditions for $Re > 5 \times 10^4$ to high accuracy. This numerical difficulty is less troublesome as P decreases. We now show critical conditions in the Prandtl number range, $10^{-5} \leqslant P \leqslant 10$, which is wider than the range $(0.3 \leqslant P \leqslant 10)$ considered by Tveitereid (1974) who used asymptotic methods.

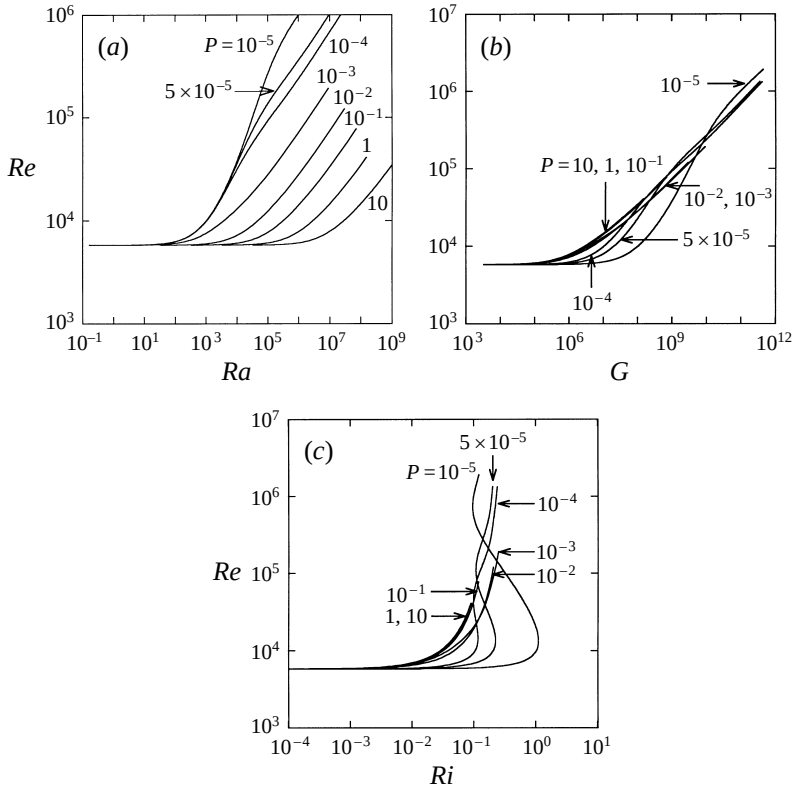

FIGURE 1. Critical Reynolds number as a function of the Rayleigh number, (*a*), the Grashof number (*b*), and the Richardson number (*c*) for different values of the Prandtl number. In (*b*), curves for $P = 10$, 1, and 0.1 are undistinguishable and curves for $P = 10^{-2}$ and 10^{-3} are undistinguishable. In (*c*), curves for $P = 10$ and 1 are undistinguishable. Note that the curves for $P \leqslant 10^{-4}$ exhibit the multi-valued situation in (*c*).

Figures 1(*a*)–1(*c*) respectively show the critical Reynolds number as a function of the Rayleigh number, Grashof number, and Richardson number for different Prandtl numbers. Here we define the Grashof number G as $G = Ra/P$. Figure 1(*a*) shows that the critical curves for $P \geqslant 0.1$ are parallel to each other for sufficiently large Ra and the horizontal distances between those three curves are almost the same. Figures 1(*b*) and 1(*c*) show that the curves for $P \geqslant 0.1$ almost coincide with each other in the (G, Re)- and (Ri, Re)-planes. Therefore the curves in the (G, Re)- or (Ri, Re)-planes for $P \geqslant 0.1$ may be regarded as the asymptotic behaviour for high Prandtl number fluids. Although figure 1(*a*) shows that the critical curves for $P = 10^{-2}$ and 10^{-3} are parallel to the curves for $P \geqslant 0.1$ and the horizontal distances between them seem to be almost the same as the distances between curves for $P \geqslant 0.1$, figures 1(*b*) and 1(*c*) show that these two cases, $P = 10^{-2}$ and 10^{-3}, exhibit different behaviour from those for $P \geqslant 0.1$ when the (Re, G)- and (Re, Ri)-planes are considered.

The low Prandtl number case, $P \leqslant 10^{-4}$, shows even more complicated characteristics. Because liquid metals typically have low values of P and are used in heat transfer applications, the low Prandtl number regime deserves attention. Figure 1(*a*) shows that three critical curves for $P = 10^{-5}$, 5×10^{-5}, and 10^{-4} coincide for $Ra < 10^3$ whereas they are well-separated for $Ra > 10^5$. The asymptotic behaviour of those curves in the high Rayleigh number limit seems to be parallel to that occurring for

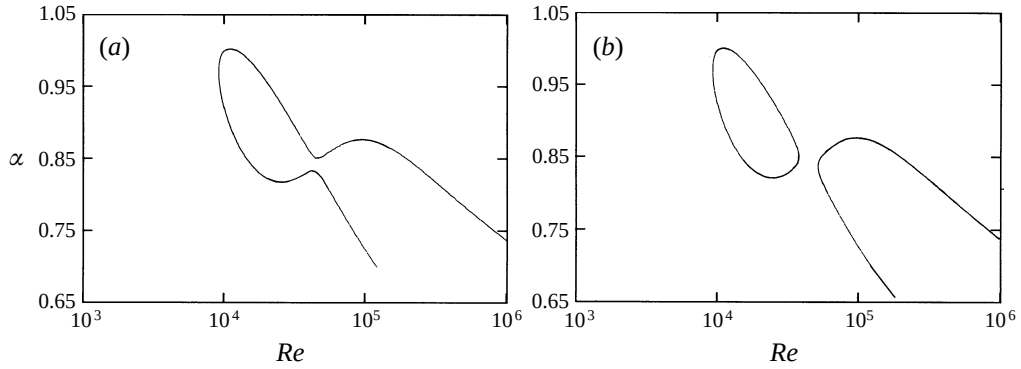

FIGURE 2. Neutral stability curve for $P = 10^{-4}$ at $Ri = 0.099$ (a) and $Ri = 0.1$ (b), just before and after the onset of the multi-valued situation shown in figure 1(c). As Ri increases further, the closed disconnected neutral curve shrinks and finally disappears, corresponding to the end of the multi-valued situation.

$P \geqslant 10^{-3}$. Actually, we may guess from figure 1(b) that the asymptotic forms of all the curves are the same for $G \to \infty$, although beyond $Re = 10^6$ it is impossible to evaluate the critical condition to high accuracy. What is unexpected is that the critical curves for $P \leqslant 10^{-4}$ are multi-valued in figure 1(c) for $0.0992 \leqslant Ri \leqslant 0.1176$ for $P = 10^{-4}$, $0.1082 \leqslant Ri \leqslant 0.2603$ for $P = 5 \times 10^{-5}$, and $0.0963 \leqslant Ri \leqslant 1.119$ for $P = 10^{-5}$. Such multi-valued situations are not observed in figure 1(a) and (b). Figures 2(a) and 2(b) show respectively the neutral stability curves for $Ri = 0.099$ and $Ri = 0.1$ at $P = 10^{-4}$, just before and after the onset of the multi-valued situation. The multi-valued situation is thus associated with the formation of a *closed disconnected neutral stability curve* as has been reported by Chen & Pearlstein (1989) and by Terrones & Pearlstein (1989) respectively for an inclined heated slot and a multicomponent fluid layer. It is important to note that the closed disconnected neutral curve is intrinsic to the use of the Richardson number where Ra is divided by P and Re^2.

Although we are focusing our attention on two-dimensional disturbances, three-dimensional ones become important between the two neutral stability curves when closed disconnected neutral stability curves exist. For the lowest value of Re_c, however, the Squire theorem is still valid.

We will discuss in the following sections the weakly nonlinear stability characteristics in the neighbourhood of these critical situations.

4. Amplitude equation and bifurcation characteristics

Here, we derive an amplitude equation based on the method of multiple scales. First we set $(\hat{\psi}, \hat{T})^T \equiv \Psi$. We expand Ψ in powers of ϵ and E where ϵ is a measure of the supercriticality defined by $Re_c^{-1} - Re^{-1} \equiv \epsilon^2 \widetilde{Re}$ with $\widetilde{Re} \sim O(1)$ and E is the critical wave component defined by $E \equiv \exp[\mathrm{i}\alpha_c(x - c_c t)]$ with the critical wavenumber α_c and the critical phase velocity c_c. We also assume that $Ri = Ri_c + \epsilon^2 \widetilde{Ri}$ with $\widetilde{Ri} \sim O(1)$ and $\alpha = \alpha_c + \epsilon^2 \tilde{\alpha}$ with $\tilde{\alpha} \sim O(1)$. The expansion is

$$\Psi = \epsilon(\Psi_{11}E + \text{c.c.}) + \epsilon^2(\Psi_{22}E^2 + \text{c.c.} + \Psi_{02}) + \epsilon^3(\Psi_{33}E^3 + \Psi_{13}E^1 + \text{c.c.}) + \epsilon^4(\Psi_{44}E^4 + \Psi_{24}E^2 + \text{c.c.} + \Psi_{04}) + \epsilon^5(\Psi_{15}E + \text{c.c.}) + O(\epsilon^5). \quad (8)$$

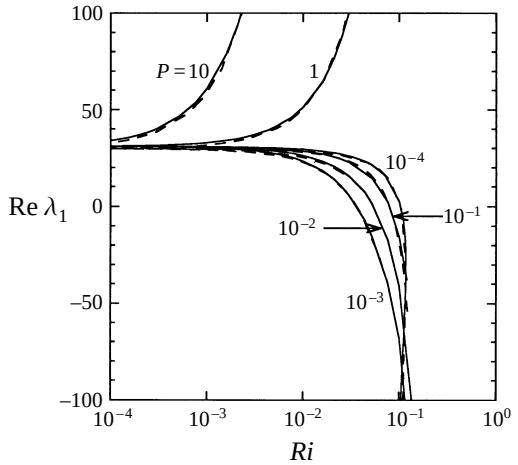

FIGURE 3. The real part of the first Landau constant, Reλ_1, changes its sign when the Prandtl number is below 0.17. All the plotted data are along the critical curves shown in figure 1. The solid curves are under the constant mass flux condition whereas the dashed curves are under the constant pressure gradient condition.

We introduce the derivative expansions

$$\partial_t = \sum_{j=0} \epsilon^{2j} \partial_{t_j}, \quad t_j = \epsilon^{2j} t. \tag{9}$$

Details of the derivation are listed in the Appendix. Let us start by listing the amplitude equation with quintic nonlinearity:

$$\mathrm{d}a/\mathrm{d}t = (\beta\lambda_0^{\alpha} + \gamma\lambda_0^{Re} + \delta\lambda_0^{Ri} + \beta^2\lambda_0^{\alpha\alpha} + \beta\gamma\lambda_0^{\alpha Re} + \beta\delta\lambda_0^{\alpha Ri} + \gamma^2\lambda_0^{ReRe} + \gamma\delta\lambda_0^{ReRi} + \delta^2\lambda_0^{RiRi})a$$
$$+(\lambda_1 + \beta\lambda_1^{\alpha} + \gamma\lambda_1^{Re} + \delta\lambda_1^{Ri})|a|^2 a + \lambda_2|a|^4 a, \tag{10}$$

where $\beta = \epsilon^2\tilde{\alpha}$, $\gamma = \epsilon^2\widetilde{Re}$, and $\delta = \epsilon^2\widetilde{Ri}$. Here, a is the amplitude of the fundamental mode defined at $z = 0$, the centreline of the channel.

4.1. *Behaviour of the cubic Landau constant* λ_1

In this subsection, we truncate the weakly nonlinear perturbation expansion (8) and (9) at the cubic-order approximation. We evaluate the cubic coefficient ('the first Landau constant' λ_1) involved in (10) for different critical sets of (P, Ri, Re). For simplicity of the analysis, the derivation of the Landau equation (Appendix) is for a constant mass flux condition. Alternatively, a constant pressure gradient condition could be used, which is relevant when we try to compare theoretical results with experimental ones. In figure 3, we plot the values of Reλ_1 in terms of *Ri* under the constant mass flux condition with solid lines and those under the constant pressure gradient condition with dashed lines. For $P > 0.17$, Reλ_1 is always positive and, for a fixed value of P, increases as *Ri* increases. This means that stable stratification, while tending to promote stability on a linear basis, also tends to increase the possibility of a subcritical instability for large values of P. We find that the real part of the first Landau constant changes its sign and becomes negative beyond some critical value of *Ri* for $P < 0.17$. The bifurcation thus changes from subcritical to supercritical when the Prandtl number is below 0.17 and the Richardson number increases beyond some critical value. This is also the case when the Rayleigh number or the Grashof

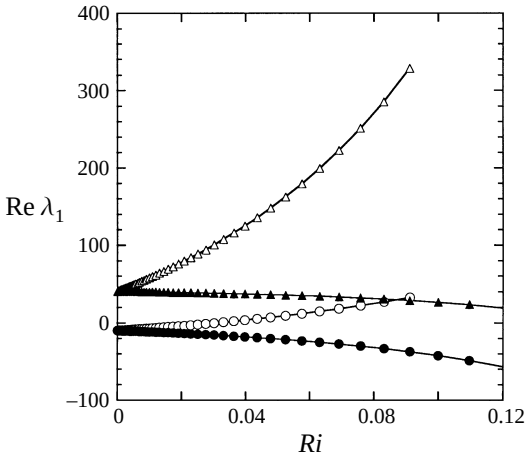

FIGURE 4. Contribution of the second harmonic $\langle N(\bar{\Phi}_{11}, \Phi_{22}) + N(\Phi_{22}, \bar{\Phi}_{11})\rangle$ and contribution of the mean-flow-distortion $\langle N(\Phi_{11}, \Phi_{02}) + N(\Phi_{02}, \Phi_{11})\rangle$ to the real part of the first Landau constant λ_1: •, the second harmonic for $P = 0.1$; ○, the second harmonic for $P = 1$; ▲, the mean-flow-distortion for $P = 0.1$; △, the mean-flow-distortion for $P = 1$.

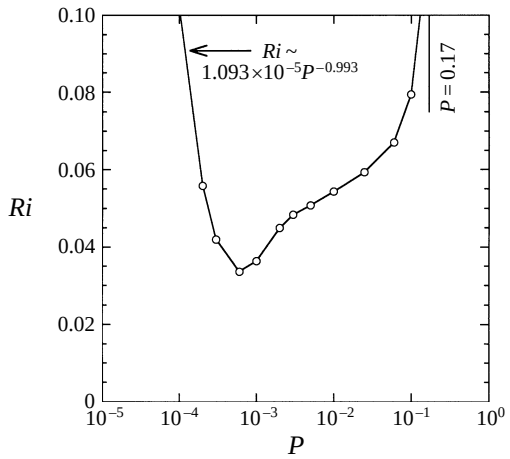

FIGURE 5. Subcritical/supercritical boundary obtained from figure 3. Above the boundary, supercritical bifurcation sets in at the linear critical points.

number increases. These figures are based on the normalization of the eigenfunction that $\phi_{11}(z = 0) = 1$. Different normalization yields different values of the Landau constants. The change from subcritical to supercritical is not affected, of course, by different normalization conditions. Both the constant mass flux condition and the constant pressure gradient condition give the same qualitative change from the subcritical situation to the supercritical one. In what follows, we will focus on the constant mass flux condition without loss of generality.

As is shown in (A6), the first Landau constant λ_1 is defined by the summation of a term resulting from the interaction between the second harmonic and the fundamental and a term resulting from the interaction between the fundamental and the mean-flow-distortion as

$$\lambda_1 = \langle N_{13}\rangle = \langle N(\bar{\Phi}_{11}, \Phi_{22}) + N(\Phi_{22}, \bar{\Phi}_{11})\rangle + \langle N(\Phi_{11}, \Phi_{02}) + N(\Phi_{02}, \Phi_{11})\rangle.$$

We show the real parts of these two terms in figure 4 for $P = 0.1$ and 1. The former term is negative while the latter is positive at $Ri = 0$. Both of these terms are increasing functions of Ri for $P = 1$ whereas they are decreasing functions of Ri for $P = 0.1$. Therefore, when P crosses 0.17 from above, these terms change from increasing to decreasing with respect to Ri.

In figure 5, we picture the boundary of the subcritical/supercritical situation in (P, Ri)-plane. Since we are examining the sign of $\mathrm{Re}\lambda_1$ at the linear critical points, (α, Re) are the critical wavenumber and the critical Reynolds number for each (P, Ri) on the curve of figure 5. From the figure, we find that the asymptotic behaviour of the boundary for small P is $Ri \sim 1.093 \times 10^{-5} P^{-0.993}$ whereas $Ri \to \infty$ for $P \to 0.17$. For values of Ri above the curve of figure 5, supercritical bifurcation occurs.

4.2. *Degenerate bifurcation*

Since the supercritical feature is obtained for relatively small Prandtl numbers, $P \leqslant 0.17$, mercury should be the best choice of fluid for showing the effects of the degeneracy at high Richardson (or Rayleigh or Grashof) number. Mercury has a Prandtl number $P = 0.025$ at room temperature. The critical condition at which the degeneracy takes place, i.e. $\mathrm{Re}\lambda_1$ vanishes, in (10) is

$$Ri = 5.9323 \times 10^{-2}, \quad Re = 12514, \quad \alpha = 0.99380, \quad c_r = 0.21136. \tag{11}$$

We evaluate all the coefficients involved in (10). The values are listed in table 1 together with the ones for $P = 10^{-4}$ and $P = 0.002832$.

Our concern here is the bifurcation of the steady solution of (10) around the degenerate point. We set $a(t) = b(t)\, \mathrm{e}^{\mathrm{i}\theta(t)}$. Equation (10) is thus written as

$$\begin{aligned} \mathrm{d}b/\mathrm{d}t &= (\beta\lambda_{0r}^{\alpha} + \gamma\lambda_{0r}^{Re} + \delta\lambda_{0r}^{Ri} + \beta^2\lambda_{0r}^{\alpha\alpha} + \beta\gamma\lambda_{0r}^{\alpha Re} + \beta\delta\lambda_{0r}^{\alpha Ri} + \gamma^2\lambda_{0r}^{ReRe} + \gamma\delta\lambda_{0r}^{ReRi} + \delta^2\lambda_{0r}^{RiRi})b \\ &\quad + (\lambda_{1r} + \beta\lambda_{1r}^{\alpha} + \gamma\lambda_{1r}^{Re} + \delta\lambda_{1r}^{Ri})b^3 + \lambda_{2r}b^5 \\ &\equiv a_0 b + a_1 b^3 + a_2 b^5, \end{aligned} \tag{12}$$

where subscript r denotes the real part. Here, λ_{0r}^{α} vanishes at the critical point and λ_{1r} vanishes at all the degenerate points, i.e. all the points on the curve of figure 5.

An existence of a nonlinear degeneracy causes an additional codimension of the bifurcation problem. Since the codimension of a local bifurcation along the line in figure 5 is two (except for a hyper-degenerate situation described later), there are two unfolding parameters, a_0 and a_1. For a prescribed a_2, we may classify the equilibrium solutions of (12) in the (a_0, a_1)-plane. For that purpose, we need to count the number of positive real roots of the bi-quadratic equation $a_0 + a_1 b^2 + a_2 b^4 = 0$. In table 2, we show how to classify the number of positive real roots, $\mathcal{N}_2$, for the general quadratic equation with real coefficients. (Complete classification of bifurcation problems with one state variable has been done by Keyfitz (1986) up to codimension seven. In the present paper, we give a useful and much handier classification in tables 2, 3, and 4.) Instead of showing a stability diagram in the (a_0, a_1)-plane, however, we prefer to discuss bifurcation characteristics in terms of the physical parameters (α, Re, Ri) based on the actual numerical coefficients obtained in table 1.

Without introducing any artificial excitation of a mode with prescribed wavenumber, all the modes belonging to the unstable wavenumber band grow simultaneously and the nonlinear evolution of such modes should be described by the Stewartson–Stuart (Ginzburg–Landau) equation instead of the Stuart–Landau equation. If, however, we introduce an artificial excitation by applying the vibrating ribbon

	$P = 0.025$	$P = 0.0001$	$P = 0.002832$
α	0.99380	0.96546	1.0090
Re	12514	9585.7	9745.1
Ri	0.059322	0.10336	0.048019
λ_{0r}^{α}	0.0	0.0	0.0
λ_{0r}^{Re}	78.499	30.211	75.488
λ_{0r}^{Ri}	−0.089281	−0.037202	−0.083690
λ_{1r}	0.0	0.0	0.0
$\lambda_{0r}^{\alpha\alpha}$	−0.20204	−0.18540	−0.20148
$\lambda_{0r}^{\alpha Re}$	−567.72	−394.94	−466.24
$\lambda_{0r}^{\alpha Ri}$	0.44911	0.075512	0.43113
λ_{0r}^{ReRe}	−364520	−424130	−292370
λ_{0r}^{ReRi}	1021.8	−221.50	872.96
λ_{0r}^{RiRi}	−0.25319	0.0057788	−0.23337
λ_{1r}^{α}	514.67	555.74	551.19
λ_{1r}^{Re}	345590	192840	499310
λ_{1r}^{Ri}	−833.00	−376.79	−1206.4
λ_{2r}	90233	−5680.7	0.0
λ_{2r}^{α}	–	–	-7.1217×10^{6}
λ_{2r}^{Re}	–	–	−0.00524
λ_{2r}^{Ri}	–	–	1.2×10^{3}
λ_{3r}^{α}	–	–	-2.2458×10^{8}
λ_{3r}^{Re}	–	–	−99.778
λ_{3r}^{Ri}	–	–	1.6422×10^{7}
β_1	–	–	0.0028964
β_2	–	–	−0.026376
λ_{4r}	–	–	-8.8065×10^{12}

TABLE 1. Coefficients involved in (10), (12), and (15)

technique, for example, we can control the frequency of the excited mode (see Nishioka, Iida & Ichikawa 1975). Since we are interested in the local bifurcation characteristics, the linear growth rate or damping rate should be negligibly small, implying that there is a one to one correspondence between the frequency and the wavenumber. Therefore, we may control the wavenumber externally. This is the reason we may consider the temporal evolution as being governed by the Stuart–Landau equation and regard the wavenumber as one of the control parameters.

According to the numerical data of table 1, $\lambda_{2r} > 0$ for $P = 0.025$. Two distinct positive roots exist if

$$a_1 < 0, \quad a_0 > 0, \quad \text{and} \quad D_2 > 0 \tag{13}$$

hold. If we require the bi-quadratic equation to have one positive and one negative root, the following should be satisfied:

$$a_0 < 0 \quad \text{and} \quad D_2 > 0. \tag{14}$$

Here, D_2 is the discriminant of a quadratic equation in table 2. Figure 6 shows subdomains for different numbers of positive real roots $\mathcal{N}_2$ in the (α, Re)-plane. It

$D_2(a_2, a_1, a_0)$	$\mathcal{N}_1(2a_2, a_1)$	a_0	$\mathcal{N}_2(a_2, a_1, a_0)$
+	1	+	2
+	0	+	0
+	*	−	1
0	1	*	1
0	0	*	0
−	*	*	0

TABLE 2. Number of positive roots $\mathcal{N}_2(a_2, a_1, a_0)$ of the quadratic equation $a_2x^2 + a_1x + a_0 = 0$ with $a_2 > 0$. Note that $\mathcal{N}_2(a_2, a_1, a_0) = \mathcal{N}_2(-a_2, -a_1, -a_0)$ for $a_2 < 0$. $\mathcal{N}_1(e_1, e_0)$ denotes the number of positive roots of $e_1x + e_0 = 0$. The discriminant $D_2(a_2, a_1, a_0)$ for the quadratic equation is defined by $D_2(a_2, a_1, a_0) = a_1^2 - 4a_0a_2$. The asterisked entry is not required to determine $\mathcal{N}_2$.

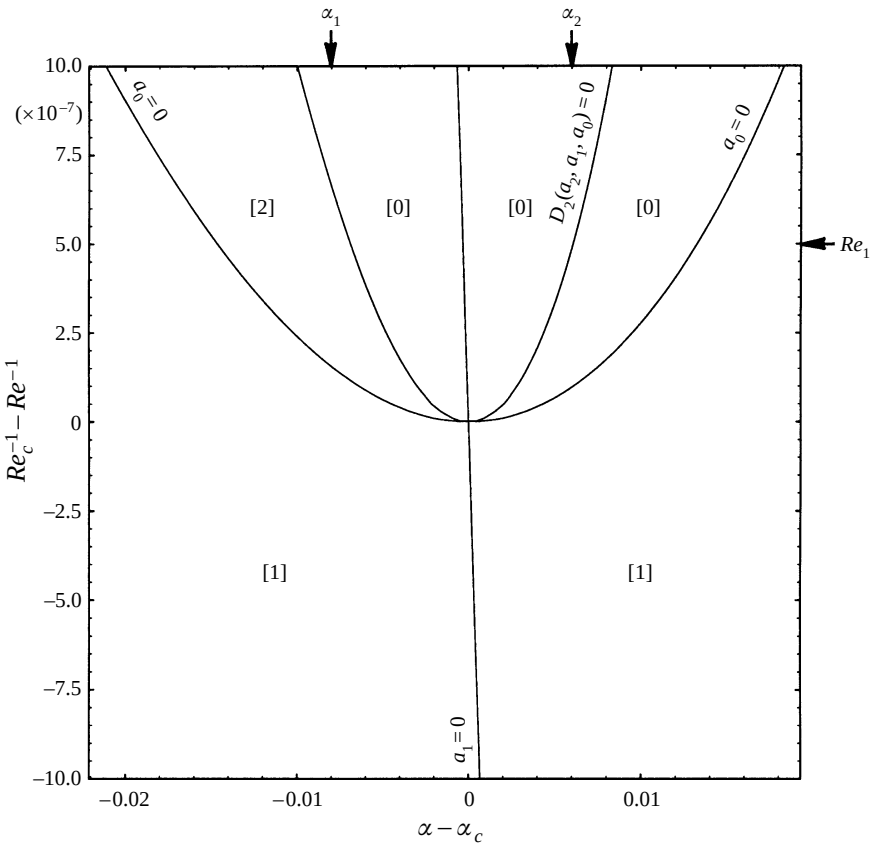

FIGURE 6. The (α, Re)-plane exhibiting curves on which entries of table 2 vanish. Each subsection has its own $\mathcal{N}_2$, the number of positive real roots of (12) for the degenerate situation with $P = 0.025$. The bracketed numerics show values of $\mathcal{N}_2$. The bifurcation diagrams in figure 7 are for $Re = Re_j$ or $\alpha = \alpha_j$ $(j = 1, 2, \cdots)$ where Re_j and α_j are indicated with arrows just outside the frame.

is convenient to discuss bifurcation characteristics along either a vertical line with fixed α or a horizontal line with prescribed Re. The two-solution state $\mathcal{N}_2 = 2$ and the one-solution state $\mathcal{N}_2 = 1$ change at criticality. Therefore, as α increases from below α_c to above, the local bifurcation characteristic changes from supercritical to

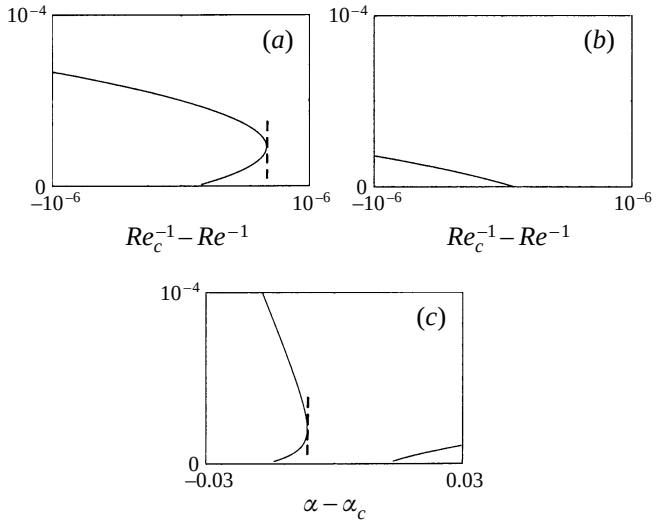

FIGURE 7. Bifurcation diagram for the degenerate situation with $Ri = 0$ and $P = 0.025$. (*a*) $\alpha - \alpha_c = -0.008$ (denoted by α_1 in figure 6), (*b*) $\alpha - \alpha_c = 0.006$ (α_2 in figure 6), (*c*) $Re_c^{-1} - Re^{-1} = 5 \times 10^{-7}$ (Re_1 in figure 6). Dashed line denotes $D_2 = 0$ in figure 6.

subcritical. Typical examples of such bifurcation characteristics are shown in figure 7 for $\delta = Ri - Ri_c = 0$. Figure 7(*b*) shows the usual subcritical bifurcation whereas figures 7(*a*) and (*c*) exhibit supercritical branches which then bend back towards the subcritical region. The upper branches of figures 7(*a*) and (*c*) are expected to bend back again towards the supercritical region. To see this, we need to carry out a fully numerical bifurcation analysis based on (3). Such a strong subcritical feature is due to the positive $\mathrm{Re}\lambda_2$. The turning points on the bifurcation diagram are located along the $D_2 = 0$ line in figure 6. For $Re > Re_c$, there are two branches as is shown in figure 7(*c*). At $Re = Re_c$, two branches merge, and for $Re < Re_c$, there is only one branch which corresponds to the unstable equilibrium solution.

A positive sign of λ_{2r} is not assumed by Eckhaus & Iooss (1989) who selected signs of coefficients so as to fit with Sen & Vashist's (1989) numerical data. We find the sign of λ_{2r} changes from positive to negative as the Prandtl number decreases along the curve of figure 5. In fact, at $P = 10^{-4}$, for example, we find that λ_{2r} is negative, consistent with the assumption of Eckhaus & Iooss. Although we do not show figures corresponding to figures 6 and 7, we can say that bifurcation characteristics change from the usual supercritical situation to a subcritical one as α increases from below α_c to above. This is due to the negative λ_{2r}. The bifurcation characteristics are similar to those obtained by Laure & Demay and Eckhaus & Iooss. Again, the turning point on the bifurcation diagram is along the $D_2 = 0$ line in the (α, Re)-plane.

Stability of the equilibrium solutions of the Stuart–Landau equation is easily inferred from table 2. For $P = 0.025$, $\lambda_{2r} > 0$. The trivial solution is unstable when $\mathcal{N}_2 = 0$ holds. The non-trivial equilibrium solution is unstable and the trivial solution is stable for $\mathcal{N}_2 = 1$. When $\mathcal{N}_2 = 2$ holds, the larger of two solutions is unstable, the smaller is stable, and the trivial solution is unstable. For $P = 10^{-4}$, on the other hand, $\lambda_{2r} < 0$ holds, and the trivial solution is stable for $\mathcal{N}_2 = 0$. The non-trivial solution is stable and the trivial solution is unstable for $\mathcal{N}_2 = 1$. When $\mathcal{N}_2 = 2$ holds, the larger of two solutions is stable, the smaller is unstable, and the trivial solution is stable.

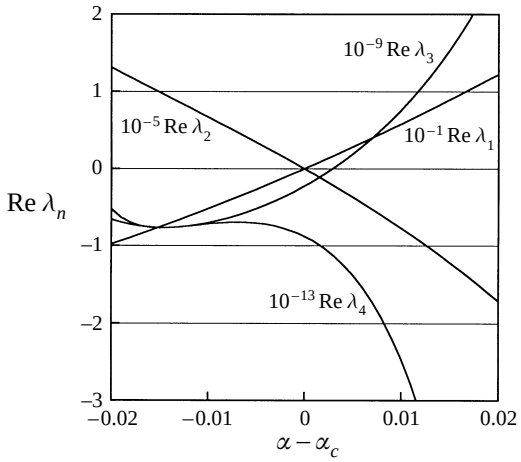

FIGURE 8. The real part of the nonlinear coefficients at $P = 0.002832$, $Re = 9745.1$, and $Ri = 0.048019$, in the neighbourhood of $\alpha = \alpha_c = 1.0090$. Note that $\mathrm{Re}\lambda_1$ and $\mathrm{Re}\lambda_2$ vanish simultaneously at $\alpha = \alpha_c$ whereas $\mathrm{Re}\lambda_3$ vanishes at $\alpha = \alpha_c + 0.0029$. The fourth Landau constant λ_4 keeps a negative real part for $\alpha \simeq \alpha_c$.

4.3. *Hyper-degeneracy*

Since we have a positive λ_{2r} at $P = 0.025$ and a negative one at $P = 10^{-4}$, λ_{2r} should change sign between these Prandtl numbers. Careful numerical computation indicates that the first and the second Landau constants, λ_1 and λ_2, lose their real parts simultaneously at criticality when $P = 0.002832$, $\alpha = 1.0090$, $Re = 9745.1$, and $Ri = 0.048019$. In figure 8, we show variations of the real parts of the Landau constants at $P = 0.002832$ as functions of $\alpha - \alpha_c$. (From the list of formula in the Appendix, it is clear that the mathematical manipulation in the weakly nonlinear reduction is getting complicated when we go to the seventh-order approximation or higher. Instead of extending the method of multiple scales, we took for computational ease an amplitude expansion method provided by Herbert (1983) in order to evaluate the higher-order numerical coefficients involved in the Stuart–Landau equation in such a hyper-degenerate situation. Both the reduction methods are guaranteed to give equivalent Stuart–Landau equations as long as the linear growth rate of the fundamental mode is small enough (Fujimura 1989).) Now we find that $\mathrm{Re}\lambda_3$ vanishes at $\alpha = \alpha_c + 0.0029$, whereas $\mathrm{Re}\lambda_4$ has a finite negative value in the neighbourhood of $\alpha = \alpha_c$. We emphasize that $\alpha - \alpha_c = 0.0029$ is very small compared with $\alpha_c = 1.0090$ so that the third Landau constant loses its real part almost simultaneously with the first and the second constants. This situation is much more 'hyper' than the Blasius boundary layer case where $\mathrm{Re}\lambda_1$ and $\mathrm{Re}\lambda_2$ do not vanish at exactly the same wavenumber. Also, because $\mathrm{Re}\lambda_3$ almost vanishes, in order let the linear term balance with a nonlinear term, we need to involve at least the ninth-order nonlinear term in the Stuart–Landau equation. Up to the quintic equation, (10) is available. We now combine the results obtained from the amplitude expansion scheme and (10). The amplitude equation involving up to the ninth-order nonlinear term is finally written as

$$\begin{aligned} \mathrm{d}a/\mathrm{d}t = {} & (\beta\lambda_0^{\alpha} + \gamma\lambda_0^{Re} + \delta\lambda_0^{Ri} + \beta^2\lambda_0^{\alpha\alpha} + \beta\gamma\lambda_0^{\alpha Re} + \beta\delta\lambda_0^{\alpha Ri} + \gamma^2\lambda_0^{ReRe} + \gamma\delta\lambda_0^{ReRi} + \delta^2\lambda_0^{RiRi})a \\ & + (\lambda_1 + \beta\lambda_1^{\alpha} + \gamma\lambda_1^{Re} + \delta\lambda_1^{Ri})|a|^2 a + (\lambda_2 + \beta\lambda_2^{\alpha} + \gamma\lambda_2^{Re} + \delta\lambda_2^{Ri})|a|^4 a \\ & + (\lambda_3^{\alpha}(\beta_1\beta_2)^{-1}(\beta - \beta_1)(\beta - \beta_2) + \gamma\lambda_3^{Re} + \delta\lambda_3^{Ri})|a|^6 a + \lambda_4|a|^8 a. \end{aligned} \tag{15}$$

$D_3(a_3,a_2,a_1,a_0)$	$\mathcal{N}_2(3a_3,2a_2,a_1)$	a_0	$\mathcal{N}_3(a_3,a_2,a_1,a_0)$
+	2	−	3
+	2,1	+	2
+	1,0	−	1
+	0	+	0
0	2	−	2
0	2	+	1
0	1	*	1
0	0	−	1
0	0	+	0
−	*	−	1
−	*	+	0

TABLE 3. Classification for the number of positive real roots $\mathcal{N}_3(a_3,a_2,a_1,a_0)$ of the cubic equation $a_3x^3+a_2x^2+a_1x+a_0=0$ with $a_3>0$. Note that $\mathcal{N}_3(a_3,a_2,a_1,a_0)=\mathcal{N}_3(-a_3,-a_2,-a_1,-a_0)$ for $a_3<0$. $\mathcal{N}_2(e_2,e_1,e_0)$ denotes the number of positive roots of $e_2x^2+e_1x+e_0=0$. The discriminant $D_3(a_3,a_2,a_1,a_0)$ for the cubic equation (17) is given by (19). The asterisked entry is not required to determine $\mathcal{N}_3$.

Again, by setting $a(t)=b(t)\,\mathrm{e}^{\mathrm{i}\theta(t)}$, we rewrite (15) as

$$\mathrm{d}b/\mathrm{d}t=(a_4b^8+a_3b^6+a_2b^4+a_1b^2+a_0)b. \tag{16}$$

We tabulate how to count the numbers of positive real roots of the cubic equation

$$a_3x^3+a_2x^2+a_1x+a_0=0, \tag{17}$$

and the quartic equation

$$a_4x^4+a_3x^3+a_2x^2+a_1x+a_0=0, \tag{18}$$

in tables 3 and 4, respectively. The discriminant $D_3(a_3,a_2,a_1,a_0)$ for the cubic equation is given by

$$D_3(a_3,a_2,a_1,a_0)=a_1^2a_2^2-4a_0a_2^3-4a_1^3a_3+18a_0a_1a_2a_3-27a_0^2a_3^2. \tag{19}$$

The discriminant $D_4(a_4,a_3,a_2,a_1,a_0)$ for the quartic equation is given by

$$\begin{aligned}D_4(a_4,a_3,a_2,a_1,a_0)&=a_1^2a_2^2a_3^2-4a_0a_2^3a_3^2-4a_1^3a_3^3+18a_0a_1a_2a_3^3-27a_0^2a_3^4-4a_1^2a_2^3a_4\\&\quad+16a_0a_2^4a_4+18a_1^3a_2a_3a_4-80a_0a_1a_2^2a_3a_4-6a_0a_1^2a_3^2a_4+144a_0^2a_2a_3^2a_4\\&\quad-27a_1^4a_4^2+144a_0a_1^2a_2a_4^2-128a_0^2a_2^2a_4^2-192a_0^2a_1a_3a_4^2+256a_0^3a_4^3.\end{aligned} \tag{20}$$

Other than $D_4(a_4,a_3,a_2,a_1,a_0)$, $D_3(4a_4,3a_3,2a_2,a_1)$, $\mathcal{N}_3(4a_4,3a_3,2a_2,a_1)$, and a_0, there are five additional parameters which affect the value of $\mathcal{N}_4(a_4,a_3,a_2,a_1,a_0)$:

$$p_1:=1 \quad \text{if} \quad q_1>0 \quad \text{and} \quad q_2>0; \quad :=0 \quad \text{otherwise}, \tag{21}$$

$$p_2=c_2^3(b_1b_2-b_0)+c_1c_2^2(b_2^2+b_1)+2c_1^2c_2b_2+c_1^3, \tag{22}$$

$$p_3=a_1-\frac{a_2a_3}{12a_4}-\frac{a_3}{2a_4}\left(\frac{5a_2}{6}-\frac{a_3^2}{4a_4}\right), \tag{23}$$

$$q_1=c_2(b_2^2-2b_1)+c_1b_2+3c_0, \tag{24}$$

$$q_2=c_2^2(b_1^2-2b_0b_2)+c_1c_2(b_1b_2-3b_0)+2c_0c_2(b_2^2-2b_1)+c_1^2b_1+2c_0c_1b_2+3c_0^2, \tag{25}$$

$\tilde{D}_4$	$\tilde{D}_3$	$\tilde{\mathcal{N}}_3$	a_0	p_1	p_2	p_3	q_1	q_2	$\mathcal{N}_4(a_4,a_3,a_2,a_1,a_0)$
+	+	3	+	0	*	*	*	*	4
+	+	3,2	−	0	*	*	*	*	3
+	+	2,1	+	0	*	*	*	*	2
+	+	1,0	−	0	*	*	*	*	1
+	+	0	+	0	*	*	*	*	0
+	+	*	*	1	*	*	*	*	0
+	0,−	*	*	*	*	*	*	*	0
0	+	3	+	*	*	*	*	−	3
0	+	2,1	+	*	+	*	*	−	2
0	+	0	+	*	*	*	*	−	0
0	+	*	−	*	+	*	*	−	1
0	+	2,1	+	*	−	*	*	−	1
0	+	*	−	*	−	*	*	−	2
0	+	3	*	*	*	*	*	0	2
0	+	2,1	*	*	*	*	*	0	1
0	+	0	*	*	*	*	*	0	0
0	+	3	+	0	*	*	−	+	3
0	+	2,3	−	0	*	*	−	+	2
0	+	1,0	−	0	*	*	−	+	1
0	+	0	+	0	*	*	−	+	0
0	+	3,2,1	*	*	+	*	+	+	1
0	+	0	*	*	+	*	+	+	0
0	+	3	*	*	−	*	+	+	1
0	+	2,1,0	*	*	−	*	+	+	0
0	0	2	*	*	*	+	+	*	1
0	0	1,0	*	*	*	+	+	*	0
0	0	2,1	*	*	*	−	+	*	1
0	0	0	*	*	*	−	+	*	0
0	0	2	+	*	*	*	−	*	2
0	0	0	+	*	*	*	−	*	0
0	0	*	−	*	*	*	−	*	1
0	−	1,0	*	*	*	*	*	*	1
−	+	3	+	*	*	*	*	*	2
−	+	2	+	*	−	*	*	*	0
−	+	2,1	+	*	+	*	*	*	2
−	+	1	+	*	−	*	*	*	0
−	+	0	+	*	*	*	*	*	0
−	0	2	+	*	*	*	*	*	2
−	0,−	0	+	*	*	*	*	*	0
−	−	1	+	*	*	*	*	*	2
−	*	*	−	*	*	*	*	*	1

TABLE 4. Classification for the number of positive roots $\mathcal{N}_4(a_4,a_3,a_2,a_1,a_0)$ of the quartic equation $a_4x^4 + a_3x^3 + a_2x^2 + a_1x + a_0 = 0$ with $a_4 > 0$. Note that $\mathcal{N}_4(a_4,a_3,a_2,a_1,a_0) = \mathcal{N}_4(-a_4,-a_3,-a_2,-a_1,-a_0)$ for $a_4 < 0$. The discriminant $\tilde{D}_4 = D_4(a_4,a_3,a_2,a_1,a_0)$ for the quartic equation (18) is given by (20). $\tilde{D}_3 = D_3(4a_4,3a_3,2a_2,a_1)$ and $\tilde{\mathcal{N}}_3 = \mathcal{N}_3(4a_4,3a_3,2a_2,a_1)$ where $\mathcal{N}_3(e_3,e_2,e_1,e_0)$ and $D_3(e_3,e_2,e_1,e_0)$ respectively denote the number of positive roots and the discriminant of $e_3x^3+e_2x^2+e_1x+e_0=0$. p_1, p_2, p_3, q_1, and q_2 are defined by (21)–(25). The asterisked entry is not required to determine $\mathcal{N}_4$.

where

$$b_2 = -\frac{3a_3}{4a_4},\ b_1 = \frac{a_2}{2a_4},\ b_0 = -\frac{a_1}{4a_4},\ c_2 = \frac{a_2}{2} - \frac{3a_3^2}{16a_4},\ c_1 = \frac{3a_1}{4} - \frac{a_2a_3}{8a_4},\ c_0 = a_0 - \frac{a_1a_3}{16a_4}.$$

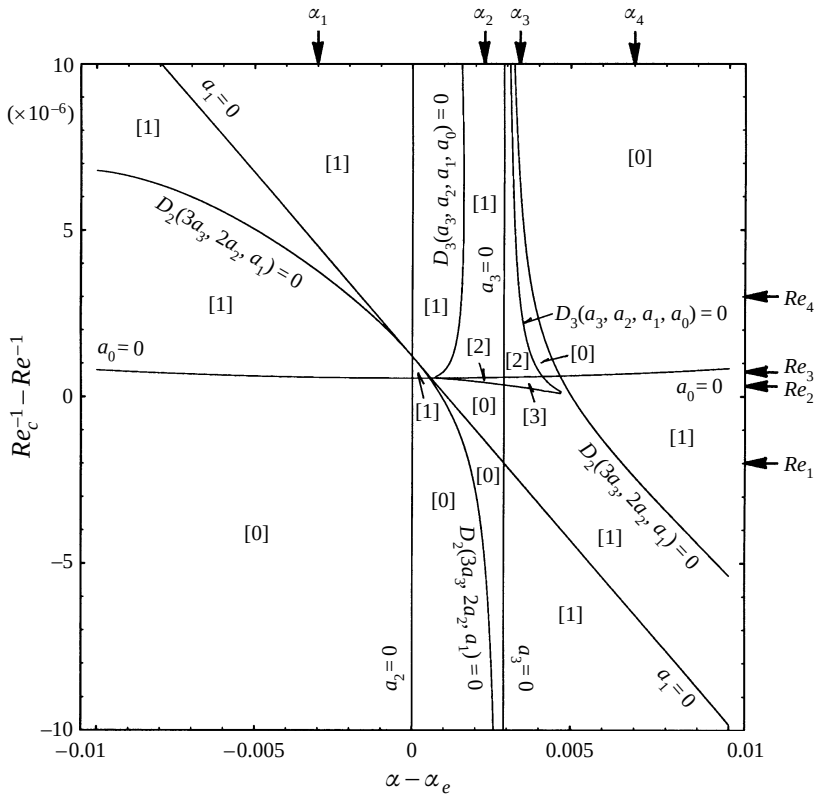

FIGURE 9. The number of positive real roots of a truncated (16) at the seventh order, $\mathcal{N}_3$, in the (α, Re)-plane for hyper-degenerate situation with $P = 0.002832$ and $\delta = 5 \times 10^{-4}$. Entries of table 3 vanish along the curves. Because of the improper truncation, the bifurcated solution diverges along $a_3 = 0$ as figure 10 demonstrates. For further description see figure 6.

In figure 9, we picture $\mathcal{N}_3$, the number of positive real roots of the bi-cubic equation which is a truncated version of (16) at the seventh order, in the (α, Re)-plane. As α increases from below α_c to above, the bifurcation diagram changes from supercritical to subcritical. Typical change of the bifurcation characteristics is shown in figure 10(*a–d*). As is inferred from figure 9 and is shown in figure 10(*e–h*), when Re increases from below Re_c to above, the bifurcated solution diverges along the $a_3 = 0$ line. All the turning points involved in figure 10 are along $D_3 = 0$ where D_3 is the discriminant of the general cubic equation defined in table 3. A similar divergence at this order has already been pointed out by Eckhaus and Iooss. Figure 9 involves a subdomain for $\mathcal{N}_3 = 3$.

Now we consider the bifurcation characteristics based on the full version of (16). Figure 11 shows $\mathcal{N}_4$, the number of positive real roots of bi-quartic equation, in the (α, Re)-plane. Across the $a_3 = 0$ line, $\mathcal{N}_4$ does not change its value. Therefore, divergence of the bifurcated solution does not occur. As α increases from below α_c to above, the bifurcation characteristic changes from supercritical to subcritical. Typical examples of the bifurcation diagram are shown in figure 12. Inclusion of the ninth-order term thus smooths out the singular behaviour on the bifurcation diagram (the same might be true in the case studied by Eckhaus & Iooss). The turning point on the bifurcation diagram is along the line $D_4 = 0$ where D_4 is the

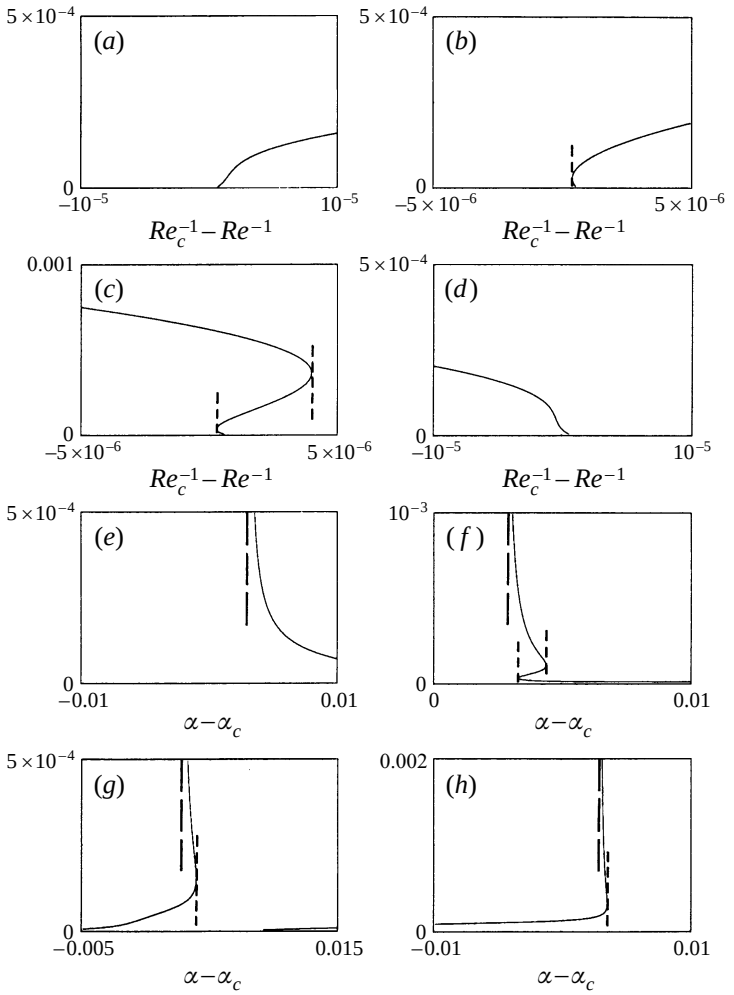

FIGURE 10. Bifurcation diagram for the hyper-degenerate situation based on the truncated equation (16) at the seventh order. (*a*) $\alpha - \alpha_c = -0.003$ (denoted by α_1 in figure 9), (*b*) $\alpha - \alpha_c = 0.0022$ (α_2 in figure 9), (*c*) $\alpha - \alpha_c = 0.0033$ (denoted by α_3 in figure 9), (*d*) $\alpha - \alpha_c = 0.007$ (α_4 in figure 9), (*e*) $Re_c^{-1} - Re^{-1} = -2 \times 10^{-6}$ (denoted by Re_1 in figure 9), (*f*) $Re_c^{-1} - Re^{-1} = 3 \times 10^{-7}$ (Re_2 in figure 9), (*g*) $Re_c^{-1} - Re^{-1} = 8 \times 10^{-7}$ (Re_3 in figure 9), (*h*) $Re_c^{-1} - Re^{-1} = 3 \times 10^{-6}$ (Re_4 in figure 9). Note that the bifurcated solution diverges along $a_3 = 0$ indicated by the long-dashed line. The turning point on the bifurcation diagram is along the line $D_3 = 0$ which is indicated by the short-dashed line where D_3 is the discriminant of the bi-cubic equation given in table 3.

discriminant of the general quartic equation as defined in table 4. The bifurcation characteristics for negative β (i.e. $\alpha < \alpha_c$) should be reproduced well even with the bi-cubic truncated system and, indeed, figure 11 and figure 9 give almost the same characteristics for negative β. The qualitative behaviour of the bifurcation diagram for $P = 10^{-4}$ is similar to that for the hyper-degenerate situation (figure 12). The $\mathcal{N}_2 = 2$ state is bounded by D_2=0 and $a_0 = 0$, and the $\mathcal{N}_2 = 1$ state exists for $a_0 > 0$ in the former. In the latter, there is no subdomain for $\mathcal{N}_4 = 3$ or 4, the $\mathcal{N}_4 = 2$ state is bounded by $D_4 = 0$ and $a_0 = 0$, and the $\mathcal{N}_4 = 1$ state exists for $a_0 > 0$ in the latter. Since $\mathrm{Re}\lambda_2 < 0$ in the former case and $\mathrm{Re}\lambda_4 < 0$ in the latter case, the highest nonlinear terms exert a stabilizing effect in both cases. This seems to be the

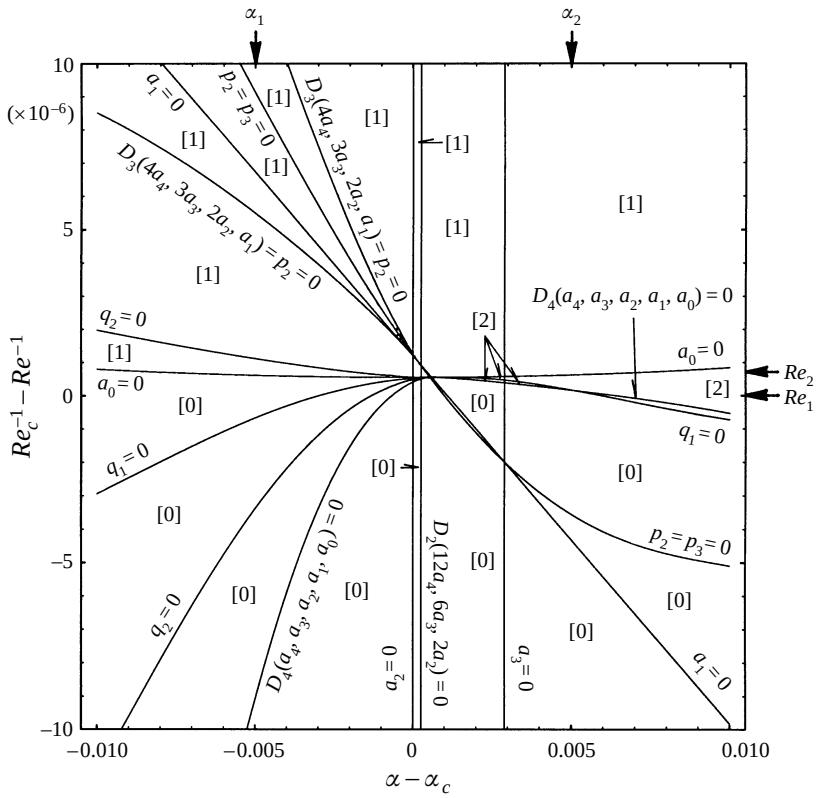

FIGURE 11. The number of positive real roots of the full version of (16) in the (α, Re)-plane for the hyper-degenerate situation, $P = 0.002832$ and $\delta = 5 \times 10^{-4}$. Entries of table 4 vanish along the curves. The ninth-order nonlinearity smooths out the divergence of the solution in figures 9 and 10. For further description see figure 6.

reason of the qualitatively similar bifurcation characteristics for $P = 10^{-4}$ and the hyper-degenerate situation.

Stability of the equilibrium solutions of the nineth-order Stuart–Landau equation is easily inferred. Since $\lambda_{4r} < 0$ holds, the trivial solution is stable for $\mathcal{N}_4 = 0$. The non-trivial solution is stable and the trivial solution is unstable for $\mathcal{N}_4 = 1$. When $\mathcal{N}_4 = 2$ holds, the larger of two solutions is stable, the smaller is unstable, and the trivial solution is stable.

5. Conclusions

Degenerate and hyper-degenerate situations are found to occur in stably stratified plane Poiseuille flow at low values of P for some particular sets of parameters. In order to illustrate the bifurcation diagram, it is useful to classify the number of positive roots of bi-quadratic, bi-cubic, and bi-quartic equations in (α, Re)-, (α, Ri)-, or (Re, Ri)-plane. The criteria for the classification are given in tables 2–4. We note here that the bifurcation diagram obtained in the present paper should be understood as a local feature. Only the small-amplitude solutions can be predicted by the amplitude equation. When the parameter set is in the neighbourhood of criticality, our results should describe bifurcation characteristics properly. In this

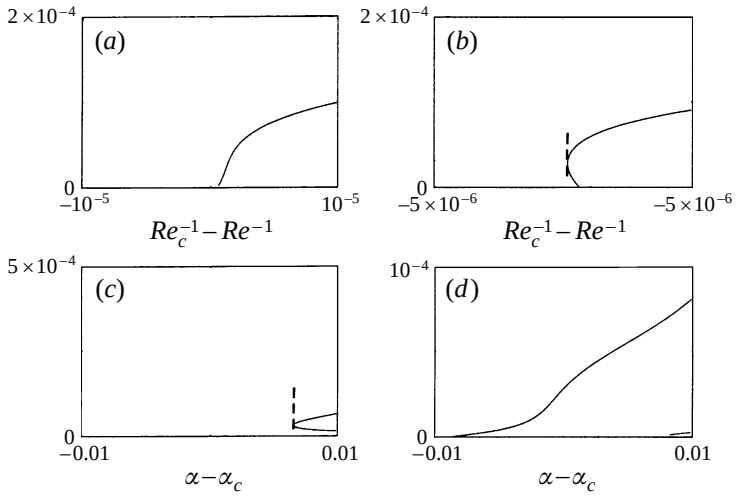

FIGURE 12. Bifurcation diagram for the hyper-degenerate situation based on the full version of (16). (*a*) $\alpha = -0.005$ (denoted by α_1 in figure 11), (*b*) $\alpha = 0.005$ (α_2 in figure 11), (*c*) $Re_c^{-1} - Re^{-1} = 0$ (Re_1 in figure 11), (*d*) $Re_c^{-1} - Re^{-1} = 7.5 \times 10^{-7}$ (Re_2 in figure 11). The turning point on the bifurcation diagram is along the $D_4 = 0$ line indicated by the dashed line, where D_4 is the discriminant of the bi-quartic equation given in table 4.

sense, we need to be careful in interpreting the upper branch of the bifurcation diagram. To make sure that a properly truncated Stuart–Landau equation gives reliable information on the bifurcation, we need to check the bifurcation features by involving still higher-order nonlinear terms in the analysis. An alternative and promising way is to check the local bifurcation characteristics with a fully numerical analysis of the bifurcation. The numerical work on this subject based on the Newton method is under development. A preliminary report has been made by Li & Fujimura (1996).

Appendix. Weakly nonlinear reduction

We apply the method of multiple scales by introducing the derivative expansions

$$\partial_t = \sum_{j=0} \epsilon^{2j} \partial_{t_j}, \quad t_j \equiv \epsilon^{2j} t. \tag{A 1}$$

For later convenience, we introduce some linear operators:

$$\boldsymbol{M}_j \equiv \begin{pmatrix} S_j & 0 \\ 0 & 1 \end{pmatrix}, \quad \boldsymbol{M}_{j,\alpha} \equiv \begin{pmatrix} -2j^2\alpha_c & 0 \\ 0 & 0 \end{pmatrix}, \quad \boldsymbol{M}_{j,\alpha\alpha} \equiv \begin{pmatrix} -2j^2 & 0 \\ 0 & 0 \end{pmatrix},$$

$$\boldsymbol{L}_j \equiv \begin{pmatrix} \mathrm{i}j\alpha_c\bar{u}S_j - \mathrm{i}j\alpha_c\bar{u}'' - Re_c^{-1}S_j^2 & \mathrm{i}j\alpha_c Ri_c \\ -\mathrm{i}j\alpha_c & \mathrm{i}j\alpha_c\bar{u} - Re_c^{-1}P^{-1}S_j \end{pmatrix},$$

$$\boldsymbol{L}_{j,Re} \equiv \begin{pmatrix} S_j^2 & 0 \\ 0 & P^{-1}S_j \end{pmatrix}, \quad \boldsymbol{L}_{j,Ri} \equiv \begin{pmatrix} 0 & \mathrm{i}j\alpha_c \\ 0 & 0 \end{pmatrix},$$

$$\boldsymbol{L}_{j,\alpha} \equiv \begin{pmatrix} \mathrm{i}j\bar{u}(S_j - 2j^2\alpha_c^2) - \mathrm{i}j\bar{u}'' + Re_c^{-1}4j^2\alpha_c S_j & \mathrm{i}jRi_c \\ -\mathrm{i}j & \mathrm{i}j\bar{u} + Re_c^{-1}P^{-1}2j^2\alpha_c \end{pmatrix},$$

$$\boldsymbol{L}_{j,\alpha\alpha} \equiv \begin{pmatrix} -6\mathrm{i}j^3\alpha_c\bar{u} - Re_c^{-1}(-4j^2\mathrm{D}^2 + 12j^4\alpha_c^2) & 0 \\ 0 & 2j^2Re_c^{-1}P^{-1} \end{pmatrix},$$

$$\boldsymbol{L}_{j,Re\alpha} \equiv \begin{pmatrix} -4j^2\alpha_c S_j & 0 \\ 0 & -2P^{-1}j^2\alpha_c \end{pmatrix}, \quad \boldsymbol{L}_{j,Ri\alpha} \equiv \begin{pmatrix} 0 & \mathrm{i}j \\ 0 & 0 \end{pmatrix},$$

where $S_j \equiv \mathrm{D}^2 - j^2\alpha_c^2$ and $\mathrm{D} \equiv \mathrm{d}/\mathrm{d}z$.

Substitute (8) as well as (A1) into (3) and equate the same powers of $\epsilon^k E^l$ to zero. We thus obtain the following system of equations. At ϵE, we have

$$[-\mathrm{i}\alpha_c c\boldsymbol{M}_1 + \boldsymbol{L}_1]\Psi_{11} = 0, \tag{A 2}$$

where the solution is expressed as

$$\Psi_{11} = A_1(t_1, t_2, \cdots)\Phi_{11}(z), \quad \Phi_{11} = \begin{pmatrix} \phi_{11}(z) \\ \theta_{11}(z) \end{pmatrix}. \tag{A 3}$$

In (A3), $A_1(t_1, t_2, \cdots)$ represents an amplitude function whose temporal evolution will be determined in the course of the reduction. Equation (A2) subject to (4) consist of the eigenvalue problem and Φ_{11} corresponds to the linear eigenfunction.

At ϵ^2E^2, ϵ^2, and ϵ^3E^3, we have the equations for the second harmonic Ψ_{22}, the mean-flow distortion Ψ_{02}, and the third harmonic Ψ_{33}, respectively, and the solutions are expressed as

$$\Psi_{22} = A_1^2\Phi_{22}(z), \quad \Psi_{02} = |A_1|^2\Phi_{02}(z), \quad \text{and} \quad \Psi_{33} = A_1^3\Phi_{33}(z). \tag{A 4}$$

At ϵ^3E, we obtain the equation for the deformation of the fundamental as

$$\begin{aligned}[-\mathrm{i}\alpha_c c\boldsymbol{M}_1 + \boldsymbol{L}_1]\Psi_{13} = \tilde{\alpha}A_1(\mathrm{i}c\boldsymbol{M}_1 + \mathrm{i}\alpha_c c\boldsymbol{M}_{1,\alpha})\Phi_{11} - A_{1,t_1}\boldsymbol{M}_1\Phi_{11} \\ -\tilde{\alpha}A_1\boldsymbol{L}_{1,\alpha}\Phi_{11} - \widetilde{Re}A_1\boldsymbol{L}_{1,Re}\Phi_{11} - \widetilde{Ri}A_1\boldsymbol{L}_{1,Ri}\Phi_{11} + |A_1|^2A_1\mathbf{N}_{13},\end{aligned} \tag{A 5}$$

where

$$\boldsymbol{N}_{13} \equiv \boldsymbol{N}(\bar{\Phi}_{11}, \Phi_{22}) + \boldsymbol{N}(\Phi_{22}, \bar{\Phi}_{11}) + \boldsymbol{N}(\Phi_{11}, \Phi_{02}) + \boldsymbol{N}(\Phi_{02}, \Phi_{11}),$$

$$\boldsymbol{N}(\Phi_{j_1,j_2}^{(j_3,j_4)}, \Phi_{k_1,k_2}^{(k_3,k_4)}) \equiv \begin{pmatrix} \mathrm{i}\alpha[j_1\phi_{j_1,j_2}^{(j_3,j_4)}S_{k_1}\mathrm{D}\phi_{k_1,k_2}^{(k_3,k_4)} - k_1\mathrm{D}\phi_{j_1,j_2}^{(j_3,j_4)}S_{k_1}\phi_{k_1,k_2}^{(k_3,k_4)}] \\ \mathrm{i}\alpha[j_1\phi_{j_1,j_2}^{(j_3,j_4)}\mathrm{D}\theta_{k_1,k_2}^{(k_3,k_4)} - k_1\mathrm{D}\phi_{j_1,j_2}^{(j_3,j_4)}\theta_{k_1,k_2}^{(k_3,k_4)}] \end{pmatrix}.$$

From the solvability condition for Ψ_{13}, we obtain

$$\begin{aligned}A_{1,t_1} &= \tilde{\alpha}\langle(\mathrm{i}c\boldsymbol{M}_1 + \mathrm{i}\alpha_c c\boldsymbol{M}_{1,\alpha} - \boldsymbol{L}_{1,\alpha})\Phi_{11}\rangle A_1 + \widetilde{Re}\langle-\boldsymbol{L}_{1,Re}\Phi_{11}\rangle A_1 \\ &\quad + \widetilde{Ri}\langle-\boldsymbol{L}_{1,Ri}\Phi_{11}\rangle A_1 + \langle\boldsymbol{N}_{13}\rangle|A_1|^2A_1 \\ &\equiv \tilde{\alpha}\lambda_0^{\alpha}A_1 + \widetilde{Re}\lambda_0^{Re}A_1 + \widetilde{Ri}\lambda_0^{Ri}A_1 + \lambda_1|A_1|^2A_1,\end{aligned} \tag{A 6}$$

where $\langle\boldsymbol{Q}(z)\rangle$ for an arbitrary smooth function $\boldsymbol{Q}(z)$ is defined by

$$\langle\boldsymbol{Q}(z)\rangle \equiv \int_{-1}^{1}\tilde{\Phi}(z)\boldsymbol{Q}(z)\mathrm{d}z \Big/ \int_{-1}^{1}\tilde{\Phi}(z)\boldsymbol{M}_1\Phi_{11}(z)\mathrm{d}z, \tag{A 7}$$

and $\tilde{\Phi}(z) = [\tilde{\phi}(z), \tilde{\theta}(z)]^T$ is an adjoint function of $\Phi(z)$ governed by

$$\begin{aligned}[\mathrm{i}\alpha_c(\bar{u} - c)S_1 + 2\mathrm{i}\alpha_c\bar{u}'\mathrm{D} - Re_c^{-1}S_1^2]\tilde{\phi} - \mathrm{i}\alpha_c\tilde{\theta} = 0, \\ \mathrm{i}\alpha_c Ri_c\tilde{\phi} + [\mathrm{i}\alpha_c(\bar{u} - c) - Re_c^{-1}P^{-1}S_1]\tilde{\theta} = 0,\end{aligned} \tag{A 8}$$

under the homogeneous boundary conditions

$$\tilde{\phi}(\pm 1) = \mathrm{D}\tilde{\phi}(\pm 1) = \tilde{\theta}(\pm 1) = 0.$$

Therefore, Ψ_{13} is obtained as

$$\Psi_{13} = \tilde{\alpha} A_1 \Phi_{13}^{(11)} + \widetilde{Re} A_1 \Phi_{13}^{(12)} + \widetilde{Ri} A_1 \Phi_{13}^{(13)} + |A_1|^2 A_1 \Phi_{13}^{(2)} + A_2 \Phi_{11}. \tag{A 9}$$

Similarly, we proceed to higher-order approximations. At $\epsilon^4 E^2$ and $\epsilon^4 E^0$, we have the equations for the second harmonic and the mean-flow-distortion at the fourth-order approximation and the solutions are written in the form of

$$\Psi_{24} = \tilde{\alpha} A_1^2 \Phi_{24}^{(11)} + \widetilde{Re} A_1^2 \Phi_{24}^{(12)} + \widetilde{Ri} A_1^2 \Phi_{24}^{(13)} + |A_1|^2 A_1^2 \Phi_{24}^{(2)} + A_1 A_2 \Phi_{24}^{(3)}, \tag{A 10}$$

$$\Psi_{04} = \tilde{\alpha} |A_1|^2 \Phi_{04}^{(11)} + \widetilde{Re} |A_1|^2 \Phi_{04}^{(12)} + \widetilde{Ri} |A_1|^2 \Phi_{04}^{(13)} + |A_1|^4 \Phi_{04}^{(2)} + \bar{A}_1 A_2 \Phi_{04}^{(3)} + A_1 \bar{A}_2 \Phi_{04}^{(4)}. \tag{A 11}$$

Finally, at $\epsilon^5 E$, we have the equation governing the deformation of the fundamental mode at the fifth-order approximation, Ψ_{15}. The solvability condition for Ψ_{15} yields

$$\begin{aligned}
A_{1,t_2} + A_{2,t_1} = {} & \tilde{\alpha}^2 A_1 \langle (\mathrm{i}c\boldsymbol{M}_1 + \mathrm{i}\alpha_c c \boldsymbol{M}_{1,\alpha}) \Phi_{13}^{(11)} + (\mathrm{i}c\boldsymbol{M}_{1,\alpha} + \tfrac{1}{2}\mathrm{i}\alpha_c c \boldsymbol{M}_{1,\alpha\alpha}) \Phi_{11} - \lambda_0^{\alpha} \boldsymbol{M}_1 \Phi_{13}^{(11)} \\
& - \lambda_0^{\alpha} \boldsymbol{M}_{1,\alpha} \Phi_{11} - \boldsymbol{L}_{1,\alpha} \Phi_{13}^{(11)} - \tfrac{1}{2} \boldsymbol{L}_{1,\alpha\alpha} \Phi_{11} \rangle \\
& + \tilde{\alpha} \widetilde{Re} A_1 \langle (\mathrm{i}c\boldsymbol{M}_1 + \mathrm{i}\alpha_c c \boldsymbol{M}_{1,\alpha}) \Phi_{13}^{(12)} - \lambda_0^{Re} \boldsymbol{M}_1 \Phi_{13}^{(11)} - \lambda_0^{\alpha} \boldsymbol{M}_1 \Phi_{13}^{(12)} \\
& - \lambda_0^{Re} \boldsymbol{M}_{1,\alpha} \Phi_{11} - \boldsymbol{L}_{1,\alpha} \Phi_{13}^{(12)} - \boldsymbol{L}_{1,Re} \Phi_{13}^{(11)} - \boldsymbol{L}_{1,Re\alpha} \Phi_{11} \rangle \\
& + \tilde{\alpha} \widetilde{Ri} A_1 \langle (\mathrm{i}c\boldsymbol{M}_1 + \mathrm{i}\alpha_c c \boldsymbol{M}_{1,\alpha}) \Phi_{13}^{(13)} - \lambda_0^{Ri} \boldsymbol{M}_1 \Phi_{13}^{(11)} - \lambda_0^{\alpha} \boldsymbol{M}_1 \Phi_{13}^{(13)} \\
& - \lambda_0^{Ri} \boldsymbol{M}_{1,\alpha} \Phi_{11} - \boldsymbol{L}_{1,\alpha} \Phi_{13}^{(13)} - \boldsymbol{L}_{1,Ri} \Phi_{13}^{(11)} - \boldsymbol{L}_{1,Ri\alpha} \Phi_{11} \rangle \\
& + \widetilde{Re}^2 A_1 \langle -\lambda_0^{Re} \boldsymbol{M}_1 \Phi_{13}^{(12)} - \boldsymbol{L}_{1,Re} \Phi_{13}^{(12)} \rangle \\
& + \widetilde{Re} \widetilde{Ri} A_1 \langle -\lambda_0^{Ri} \boldsymbol{M}_1 \Phi_{13}^{(12)} - \lambda_0^{Re} \boldsymbol{M}_1 \Phi_{13}^{(13)} - \boldsymbol{L}_{1,Ri} \Phi_{13}^{(12)} - \boldsymbol{L}_{1,Re} \Phi_{13}^{(13)} \rangle \\
& + \widetilde{Ri}^2 A_1 \langle -\lambda_0^{Ri} \boldsymbol{M}_1 \Phi_{13}^{(13)} - \boldsymbol{L}_{1,Ri} \Phi_{13}^{(13)} \rangle \\
& + \tilde{\alpha} |A_1|^2 A_1 \langle (\mathrm{i}c\boldsymbol{M}_1 + \mathrm{i}\alpha_c c \boldsymbol{M}_{1,\alpha}) \Phi_{13}^{(2)} - \lambda_1 \boldsymbol{M}_1 \Phi_{13}^{(11)} \\
& - (2\lambda_0^{\alpha} + \bar{\lambda}_0^{\alpha}) \boldsymbol{M}_1 \Phi_{13}^{(2)} - \lambda_1 \boldsymbol{M}_{1,\alpha} \Phi_{11} - \boldsymbol{L}_{1,\alpha} \Phi_{13}^{(2)} + \mathbf{N}_{15}^{(11)} \rangle \\
& + \tilde{\alpha} A_2 \langle (\mathrm{i}c\boldsymbol{M}_1 + \mathrm{i}\alpha_c c \boldsymbol{M}_{1,\alpha}) \Phi_{11} - \boldsymbol{L}_{1,\alpha} \Phi_{11} \rangle \\
& + \widetilde{Re} |A_1|^2 A_1 \langle -\lambda_1 \boldsymbol{M}_1 \Phi_{13}^{(12)} - (2\lambda_0^{Re} + \bar{\lambda}_0^{Re}) \boldsymbol{M}_1 \Phi_{13}^{(2)} - \boldsymbol{L}_{1,Re} \Phi_{13}^{(2)} + \mathbf{N}_{15}^{(12)} \rangle \\
& + \widetilde{Re} A_2 \langle -\boldsymbol{L}_{1,Re} \Phi_{11} \rangle + \widetilde{Ri} A_2 \langle -\boldsymbol{L}_{1,Ri} \Phi_{11} \rangle \\
& + \widetilde{Ri} |A_1|^2 A_1 \langle -\lambda_1 \boldsymbol{M}_1 \Phi_{13}^{(13)} - (2\lambda_0^{Ri} + \bar{\lambda}_0^{Ri}) \boldsymbol{M}_1 \Phi_{13}^{(2)} - \boldsymbol{L}_{1,Ri} \Phi_{13}^{(2)} + \mathbf{N}_{15}^{(13)} \rangle \\
& + |A_1|^4 A_1 \langle -(2\lambda_1 + \bar{\lambda}_1) \boldsymbol{M}_1 \Phi_{13}^{(2)} + \mathbf{N}_{15}^{(2)} \rangle + |A_1|^2 A_2 \langle \mathbf{N}_{15}^{(3)} \rangle + A_1^2 \bar{A}_2 \langle \mathbf{N}_{15}^{(4)} \rangle \\
\equiv {} & \tilde{\alpha}^2 A_1 \lambda_0^{\alpha\alpha} + \tilde{\alpha} \widetilde{Re} A_1 \lambda_0^{\alpha Re} + \tilde{\alpha} \widetilde{Ri} A_1 \lambda_0^{\alpha Ri} + \widetilde{Re}^2 A_1 \lambda_0^{ReRe} \\
& + \widetilde{Re} \widetilde{Ri} A_1 \lambda_0^{ReRi} + \widetilde{Ri}^2 A_1 \lambda_0^{RiRi} + \tilde{\alpha} |A_1|^2 A_1 \lambda_1^{\alpha} + \widetilde{Re} |A_1|^2 A_1 \lambda_1^{Re} \\
& + \widetilde{Ri} |A_1|^2 A_1 \lambda_1^{Ri} + \lambda_2 |A_1|^4 A_1 + \tilde{\alpha} A_2 \lambda_0^{\alpha} + \widetilde{Re} A_2 \lambda_0^{Re} + \widetilde{Ri} A_2 \lambda_0^{Ri} \\
& + 2\lambda_1 |A_1|^2 A_2 + \lambda_1 A_1^2 \bar{A}_2.
\end{aligned} \tag{A 12}$$

Here nonlinear terms are defined by

$$\begin{aligned}
\boldsymbol{N}_{15}^{(11)} &= \boldsymbol{N}(\boldsymbol{\Phi}_{13}^{(11)}, \boldsymbol{\Phi}_{02}) + \boldsymbol{N}(\boldsymbol{\Phi}_{02}, \boldsymbol{\Phi}_{13}^{(11)}) + \boldsymbol{N}(\bar{\boldsymbol{\Phi}}_{13}^{(11)}, \boldsymbol{\Phi}_{22}) + \boldsymbol{N}(\boldsymbol{\Phi}_{22}, \bar{\boldsymbol{\Phi}}_{13}^{(11)}) \\
&\quad + \boldsymbol{N}(\boldsymbol{\Phi}_{04}^{(11)}, \boldsymbol{\Phi}_{11}) + \boldsymbol{N}(\boldsymbol{\Phi}_{11}, \boldsymbol{\Phi}_{04}^{(11)}) + \boldsymbol{N}(\boldsymbol{\Phi}_{24}^{(11)}, \bar{\boldsymbol{\Phi}}_{11}) + \boldsymbol{N}(\bar{\boldsymbol{\Phi}}_{11}, \boldsymbol{\Phi}_{24}^{(11)}) \\
&\quad + \boldsymbol{N}_{\alpha}(\boldsymbol{\Phi}_{11}, \boldsymbol{\Phi}_{02}) + \boldsymbol{N}_{\alpha}(\boldsymbol{\Phi}_{02}, \boldsymbol{\Phi}_{11}) + \boldsymbol{N}_{\alpha}(\bar{\boldsymbol{\Phi}}_{11}, \boldsymbol{\Phi}_{22}) + \boldsymbol{N}_{\alpha}(\boldsymbol{\Phi}_{22}, \bar{\boldsymbol{\Phi}}_{11}), \\
\boldsymbol{N}_{15}^{(12)} &= \boldsymbol{N}(\boldsymbol{\Phi}_{13}^{(12)}, \boldsymbol{\Phi}_{02}) + \boldsymbol{N}(\boldsymbol{\Phi}_{02}, \boldsymbol{\Phi}_{13}^{(12)}) + \boldsymbol{N}(\bar{\boldsymbol{\Phi}}_{13}^{(12)}, \boldsymbol{\Phi}_{22}) + \boldsymbol{N}(\boldsymbol{\Phi}_{22}, \bar{\boldsymbol{\Phi}}_{13}^{(12)}) \\
&\quad + \boldsymbol{N}(\boldsymbol{\Phi}_{04}^{(12)}, \boldsymbol{\Phi}_{11}) + \boldsymbol{N}(\boldsymbol{\Phi}_{11}, \boldsymbol{\Phi}_{04}^{(12)}) + \boldsymbol{N}(\boldsymbol{\Phi}_{24}^{(12)}, \bar{\boldsymbol{\Phi}}_{11}) + \boldsymbol{N}(\bar{\boldsymbol{\Phi}}_{11}, \boldsymbol{\Phi}_{24}^{(12)}), \\
\boldsymbol{N}_{15}^{(13)} &= \boldsymbol{N}(\boldsymbol{\Phi}_{13}^{(13)}, \boldsymbol{\Phi}_{02}) + \boldsymbol{N}(\boldsymbol{\Phi}_{02}, \boldsymbol{\Phi}_{13}^{(13)}) + \boldsymbol{N}(\bar{\boldsymbol{\Phi}}_{13}^{(13)}, \boldsymbol{\Phi}_{22}) + \boldsymbol{N}(\boldsymbol{\Phi}_{22}, \bar{\boldsymbol{\Phi}}_{13}^{(13)}) \\
&\quad + \boldsymbol{N}(\boldsymbol{\Phi}_{04}^{(13)}, \boldsymbol{\Phi}_{11}) + \boldsymbol{N}(\boldsymbol{\Phi}_{11}, \boldsymbol{\Phi}_{04}^{(13)}) + \boldsymbol{N}(\boldsymbol{\Phi}_{24}^{(13)}, \bar{\boldsymbol{\Phi}}_{11}) + \boldsymbol{N}(\bar{\boldsymbol{\Phi}}_{11}, \boldsymbol{\Phi}_{24}^{(13)}), \\
\boldsymbol{N}_{15}^{(2)} &= \boldsymbol{N}(\boldsymbol{\Phi}_{33}, \bar{\boldsymbol{\Phi}}_{22}) + \boldsymbol{N}(\bar{\boldsymbol{\Phi}}_{22}, \boldsymbol{\Phi}_{33}) + \boldsymbol{N}(\boldsymbol{\Phi}_{13}^{(2)}, \boldsymbol{\Phi}_{02}) + \boldsymbol{N}(\boldsymbol{\Phi}_{02}, \boldsymbol{\Phi}_{13}^{(2)}) \\
&\quad + \boldsymbol{N}(\bar{\boldsymbol{\Phi}}_{13}^{(2)}, \boldsymbol{\Phi}_{22}) + \boldsymbol{N}(\boldsymbol{\Phi}_{22}, \bar{\boldsymbol{\Phi}}_{13}^{(2)}) + \boldsymbol{N}(\boldsymbol{\Phi}_{04}^{(2)}, \boldsymbol{\Phi}_{11}) + \boldsymbol{N}(\boldsymbol{\Phi}_{11}, \boldsymbol{\Phi}_{04}^{(2)}) \\
&\quad + \boldsymbol{N}(\boldsymbol{\Phi}_{24}^{(2)}, \bar{\boldsymbol{\Phi}}_{11}) + \boldsymbol{N}(\bar{\boldsymbol{\Phi}}_{11}, \boldsymbol{\Phi}_{24}^{(2)}), \\
\boldsymbol{N}_{15}^{(3)} &= 2\boldsymbol{N}_{13}, \quad \boldsymbol{N}_{15}^{(4)} = \boldsymbol{N}_{13},
\end{aligned}$$

and

$$\boldsymbol{N}_{\alpha}(\boldsymbol{\Phi}_{j_1,j_2}, \boldsymbol{\Phi}_{k_1,k_2}) \equiv \begin{pmatrix} \mathrm{i}[j_1 \phi_{j_1,j_2} S_{k_1} \mathrm{D}\phi_{k_1,k_2} - k_1 \mathrm{D}\phi_{j_1,j_2} S_{k_1} \phi_{k_1,k_2}] \\ +\mathrm{i}\alpha_c[-2j_1 k_1^2 \alpha_c \phi_{j_1,j_2} \mathrm{D}\phi_{k_1,k_2} + 2k_1^3 \alpha_c \mathrm{D}\phi_{j_1,j_2} \phi_{k_1,k_2}] \\ \\ \mathrm{i}[j_1 \phi_{j_1,j_2} \mathrm{D}\theta_{k_1,k_2} - k_1 \mathrm{D}\phi_{j_1,j_2} \theta_{k_1,k_2}] \end{pmatrix}.$$

Summing (A6) and (A12) after multiplying ϵ^3 and ϵ^5, respectively, letting $a \equiv \epsilon A_1 + \epsilon^3 A_2 + \cdots$, and setting $\beta \equiv \epsilon^2 \tilde{\alpha}$, $\gamma \equiv \epsilon^2 \widetilde{Re}$ and $\delta \equiv \epsilon^2 \widetilde{Ri}$, we obtain the amplitude equation for a as

$$\begin{aligned}
\mathrm{d}a/\mathrm{d}t &= (\beta\lambda_0^{\alpha} + \gamma\lambda_0^{Re} + \delta\lambda_0^{Ri} + \beta^2\lambda_0^{\alpha\alpha} + \beta\gamma\lambda_0^{\alpha Re} + \beta\delta\lambda_0^{\alpha Ri} + \gamma^2\lambda_0^{ReRe} + \gamma\delta\lambda_0^{ReRi} + \delta^2\lambda_0^{RiRi})a \\
&\quad + (\lambda_1 + \beta\lambda_1^{\alpha} + \gamma\lambda_1^{Re} + \delta\lambda_1^{Ri})|a|^2 a + \lambda_2 |a|^4 a. \qquad \text{(A 13)}
\end{aligned}$$

REFERENCES

Chen, Y.-M. & Pearlstein, A. J. 1989 *J. Fluid Mech.* **198**, 513.
Eckhaus, W. & Iooss, G. 1989 *Physica* D **39**, 124.
Fujimura, K. 1989 *Proc. R. Soc. Lond.* A **424**, 373.
Fujimura, K. & Kelly, R. E. 1995 *Phys. Fluids* **7**, 68.
Gage, K. S. & Reid, W. H. 1968 *J. Fluid Mech.* **33**, 21.
Herbert, T. 1980 *AIAA J.* **18**, 243.
Herbert, T. 1983 *J. Fluid Mech.* **126**, 167.
Keyfitz, B. L. 1986 *Dyn. Stability Systems* **1**, 1.
Kirillov, I. R., Reed, C. B. & Barleon, L. 1995 *Fusion Engng Design* **27**, 553.
Knobloch, E. 1986 *Contemp. Math* **56**, 193.
Laure, P. & Demay, Y. 1988 *Computers Fluids* **16**, 229.
Li, H.-S. & Fujimura, K. 1996 *Phys. Fluids* **8**, 1127.
Nishioka, M., Iida, S. & Ichikawa, Y. 1975 *J. Fluid Mech.* **72**, 731.
Pekeris, C. L. & Shkoller, B. 1967 *J. Fluid Mech.* **29**, 31.
Reynolds, W. C. & Potter, M. C. 1967 *J. Fluid Mech.* **27**, 465.
Sen, P. K. & Vashist, T. K. 1989 *Proc. R. Soc. Lond.* A **424**, 81.
Terrones, G. & Pearlstein, A. J. 1989 *Phys. Fluids* A **1**, 845.
Tveitereid, M. 1974 *Z. Angew. Math. Mech.* **54**, 533.